



OPEN ACCESS

Edited by:Rawil Fakhru'llin,
Kazan Federal University, Russia**Reviewed by:**Dan Shao,
South China University of Technology,
China

Tsong-Rong Kuo,

Taipei Medical University, Taiwan

Hamed Barabadi,

Shahid Beheshti University of Medical
Sciences, Iran

Ehsan Nazarzadeh Zare,

Damghan University, Iran

Pengfei Zhang,

Shenzhen Institutes of Advanced
Technology, (CAS), China

Li-Xing Yang,

National Cheng Kung University,
Taiwan

Hemant Kumar Daima,

Amity University Jaipur, India

Mei-Yi Liao,

National Pingtung University, Taiwan

***Correspondence:**

Tingting Zhao

ttzhao@ahmu.edu.cn

Weijun Fang

fangweijun@ahmu.edu.cn

[†]These authors have contributed
equally to this work**Specialty section:**This article was submitted to
Nanobiotechnology,
a section of the journal
Frontiers in Bioengineering and
Biotechnology**Received:** 14 February 2022**Accepted:** 02 June 2022**Published:** 19 July 2022**Citation:**Zhang H, Xu J, Zhang X, Wang T,
Zhou D, Shu W, Zhao T and Fang W
(2022) One-Pot Synthesis of Ag/
Quaternary Ammonium Salt Co-
Decorated Mesoporous Silica
Nanoparticles for Synergistic
Treatment of Cancer and
Bacterial Infections.
Front. Bioeng. Biotechnol. 10:875317.
doi: 10.3389/fbioe.2022.875317

One-Pot Synthesis of Ag/Quaternary Ammonium Salt Co-Decorated Mesoporous Silica Nanoparticles for Synergistic Treatment of Cancer and Bacterial Infections

Hanyuan Zhang^{1†}, Jianxiang Xu^{2†}, Xu Zhang², Teng Wang², Dairan Zhou², Wei Shu², Tingting Zhao^{2*} and Weijun Fang^{2*}¹Department of Orthopedics, Department of Sports Medicine and Arthroscopic Surgery, The First Affiliated Hospital of Anhui Medical University, Hefei, China, ²School of Basic Medical Sciences, Anhui Medical University, Hefei, China

Developing drug delivery nanosystems with both anticancer and antibacterial effects is of great clinical value. Herein, we report a facile approach to synthesize Ag and quaternary ammonium salt (QAS) co-decorated mesoporous silica nanoparticles (MSNs), namely, Ag/QAS-MSNs, for synergistic treatment of cancer and bacterial infections. *In vitro* studies demonstrated that Ag/QAS-MSNs not only had a strong antibacterial activity against the bacterial pathogens but also could efficiently induce cancer cell death through an apoptotic pathway. Moreover, *in vivo* combination therapy with Ag and QAS in Ag/QAS-MSNs was also tested in a nude mouse tumor model, and a significant synergistic anticancer effect, which is superior to that obtained by therapy with Ag-MSNs or QAS-MSNs alone, was achieved. Such excellent anticancer and antibacterial activity of Ag/QAS-MSNs could be attributed to the synergistic effect of Ag ions and QAS. Thus, Ag/QAS-MSNs have a promising future as potent anticancer agents with high antibacterial performance.

Keywords: synergistic treatment, anticancer, antibacterial activity, mesoporous silica nanoparticles, quaternary ammonium salts, Ag

1 INTRODUCTION

Cancer is a life-threatening disease with a great worldwide impact. According to statistics, approximately 19.29 million new cancer cases and 9.96 million cancer deaths have occurred in 2020 worldwide (Siegel et al., 2020). At present, chemotherapy, surgery, and radiotherapy are still the three dominant treatment approaches. However, owing to drug resistance and lacking targeted ability, most cancer patients often have a poor prognosis. Moreover, numerous studies have shown that cancer-associated bacteria can seriously reduce the efficiency of cancer treatments (Wallace et al., 2010; Dewerd, 2015; Liang et al., 2017; Yougbare et al., 2019). For instance, some bacteria in the tumor microenvironment can metabolize chemotherapeutic drugs or regulate the autophagy of tumor cells, resulting in enhanced tumor cells becoming resistant to chemo-drugs (Geller et al., 2017; Yu et al., 2017). Meanwhile, cancer patients with a weakened immune system are more susceptible to bacterial infections (Bullman et al., 2017; Harper, 2019). To address these challenges, the development of a new strategy based on a single element for both treating cancer and killing bacteria is of great clinical significance.

As is well known, quaternary ammonium salts (QASs) are composed of a hydrophilic ammonium cation head and a hydrophobic alkyl tail. Based on this unique structure, QASs can adhere to the negatively charged cellular membrane of microorganisms by electrostatic interaction, and then the hydrophobic alkyl tail can incorporate into the membrane lipid bilayer, resulting in cell membrane damage or cell membrane protein denaturation. Hence, QASs are bactericidal and fungicidal, as well as active toward tumor cells (He et al., 2010; Banerjee et al., 2011; He et al., 2011; Oblak et al., 2019; Kwasniewska et al., 2020; Tang et al., 2020; He et al., 2021). To date, several groups have demonstrated that the QAS could be used as a potential cancer-specific compound against head and neck cancer cell lines (Ito et al., 2009; Meena et al., 2017). In addition to, several nanoparticle-based systems also exhibited both anticancer and antibacterial abilities, such as iron oxide nanoparticles and carbon-related materials (Chu et al., 2013; Huang et al., 2015; Yu and Chi, 2020; Bayda et al., 2021; Te and Wei, 2022). In contrast, silver (Ag) nanoparticles possess a remarkable antibacterial and anticancer activity and have been widely used in medicine with significant applications including antimicrobial, bioimaging, and cancer therapy (Tang and Zheng, 2018; Deshmukh et al., 2019; Ahn and Park, 2020; Eid et al., 2020; Xu et al., 2020; Hsu et al., 2021; Bi et al., 2022). Compared to conventional anticancer drugs, QASs and Ag nanoparticles are cheaper and easier to use. These advantages make QASs and Ag nanoparticles as promising cancer therapeutic candidates.

A way to improve the efficacy of anticancer treatment is by the dual loading of drugs on a single nanovehicle, exploiting the synergetic effect of drugs (Oliveira et al., 2016; Kang et al., 2018; Montalvo-Quiros et al., 2019; Chen et al., 2020; Lima-Sousa et al., 2020; Song et al., 2020; Tan et al., 2020; Shen et al., 2021; Galhano et al., 2022). However, developing a dual drug-loaded nanosystem still remains a significant challenge. Herein, we designed a facile one-pot route to fabricate Ag and QAS co-decorated mesoporous silica nanoparticles (MSNs) (Ag/QAS-MSNs) for simultaneous fighting cancer and bacterial infections. The synthesized nanoparticles were characterized to study their physico-chemical properties using transmission electron microscopy (TEM), scanning electron microscopy (SEM), X-ray diffraction (XRD), energy dispersive spectroscopy, Fourier transform infrared spectroscopy (FTIR), and thermogravimetric analysis (TGA). We also thoroughly tested their anticancer *in vitro* and antibacterial activity against pathogenic Gram-negative (*Escherichia coli* JM109) and Gram-positive strains (*Staphylococcus aureus*). Moreover, the therapeutic effect and biosafety of Ag/QAS-MSNs were further studied *in vivo*.

2 EXPERIMENTAL SECTION

2.1 Materials and Methods

Tetraethylorthosilicate (TEOS, Alfa Aesar, United States), N-(aminoethyl)-amino-propyl trimethoxysilane (TSD, Alfa Aesar, United States), silver nitrate (AgNO_3 , Aladdin, China), hexadecyltrimethylammonium hydroxide salt (CTA-OH, 10% in water, Aladdin, China), formalin (HCHO, 40%, Sinopharm,

China) ammonium nitrate (NH_4NO_3 , Sinopharm, China), ammonium aqueous solution ($\text{NH}_3\cdot\text{H}_2\text{O}$, 25%, Sinopharm, China), methanol (CH_3OH , Sinopharm, China), and ethanol ($\text{C}_2\text{H}_5\text{OH}$, Sinopharm, China) were used as received without further purification. The bacterial strains (*Escherichia coli* JM109 and *Staphylococcus aureus*) were obtained from the Department of Microbiology, Anhui Medical University (China).

2.2 Instruments and Characteristics

SEM images and EDX spectra were captured on a Hitachi S4800 scanning electron microscope. TEM images were captured on a TECNAI F-30 high-resolution transmission electron microscope. XRD data were obtained in a PANalytical X'Pert diffractometer with Cu-K α radiation from 10° to 80°. The concentrations of silver ions were tested using an inductively coupled plasma-atomic emission spectrophotometer (ICP-AES, IRIS Intrepid II XSP). The surface properties of the samples were determined using FTIR spectrum (Perkin-Elmer, Spectrum spectrometer), zeta potential (Nano ZS & MPT-2, Malvern), surface area, and pore size (Micromeritics Instrument Corp. ASAP 2020). Fluorescence micrographs were obtained on an Olympus IX71 fluorescence microscope.

2.3 Preparation of Ag/QAS Co-Decorated Mesoporous Silica Nanoparticles (Ag/QAS-MSNs)

The MSNs co-decorated with Ag nanoparticles and hexadecyltrimethylammonium hydroxide salts were prepared via a one-pot method (Tian et al., 2014) (Figure 1A). A solution of CTA-OH (10% in water, 3.0 ml) and water (80.0 ml) was preheated to 80°C. Then, 0.833 ml of TEOS in ethanol (5.0 ml) and 0.25 ml of TSD and 30 mg of AgNO_3 in water (2.0 ml) were simultaneously added into the above solution with stirring for 2 h. Further, 2 ml of formalin was added into the mixture with stirring for an additional 1 h at 80°C to reduce the loaded Ag ions into Ag nanoparticles. The final products were washed by ethanol and water for several times and dried in an oven at 50°C overnight.

2.4 Removal of Quaternary Ammonium Salts From Ag/QAS Co-Decorated Mesoporous Silica Nanoparticles

Ag/QAS-MSNs were dispersed in 10 ml of NH_4NO_3 ethanol solution (20 mg/ml) (Fang et al., 2012). The mixture was heated to 45°C under stirring for 4 h, and then the products (Ag-MSNs) were collected by centrifugation and washed with ethanol several times. The procedures were repeated three times.

2.5 Removal of Ag Nanocrystals From Ag/Quaternary Ammonium Salts Co-Decorated Mesoporous Silica Nanoparticles

The removal of the Ag nanocrystals from Ag/QAS-MSNs was performed by adding Ag/QAS-MSNs in a solution of water (1.0 ml) and $\text{NH}_3\cdot\text{H}_2\text{O}$ (100 μl , 25%) followed by stirring at

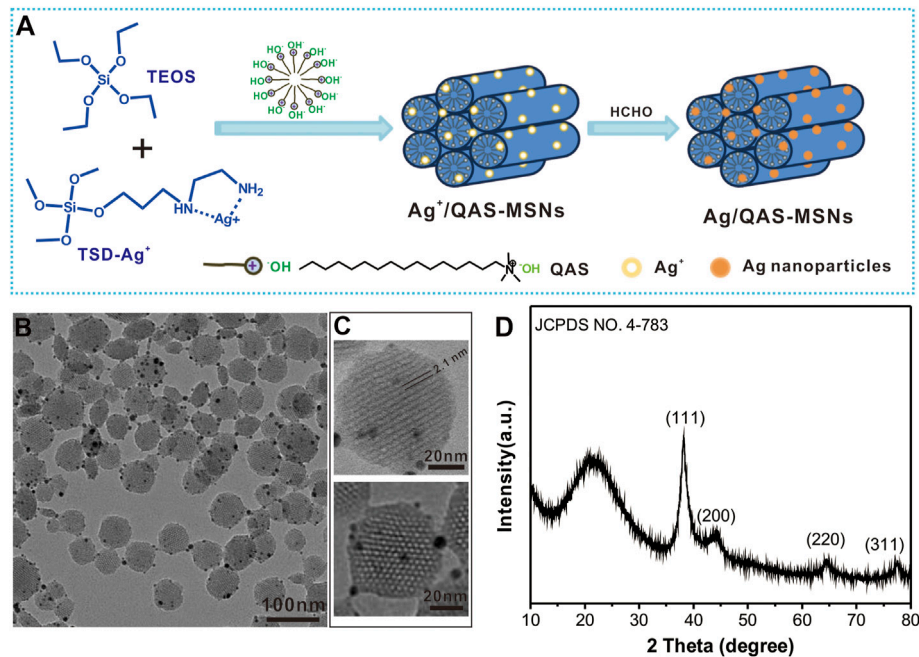


FIGURE 1 | (A) Schematic illustration for the synthesis of Ag/QAS co-decorated MSNs. (B) TEM image of Ag/QAS-MSNs. (C) HRTEM images of Ag/QAS-MSNs. (D) XRD patterns of Ag/QAS-MSNs.

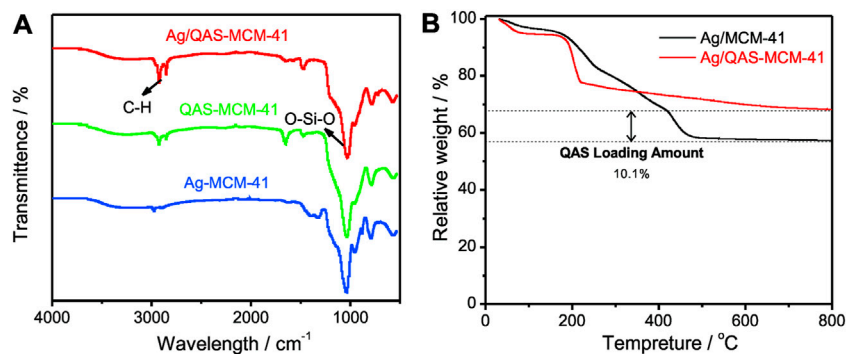


FIGURE 2 | (A) FTIR spectra of Ag/QAS-MSNs, QAS-MSNs, and Ag-MSNs. (B) Thermogravimetric analysis (TGA) curves of Ag/QAS-MSNs and MSNs.

room temperature for 15 min. The obtained QAS-MSNs were washed with water for several times. To obtain MSNs, both Ag nanocrystals and QAS molecules in Ag/QAS-MSNs were removed using the above method.

2.6 Fourier Transform Infrared Spectroscopy Tests

The samples were collected by centrifugation, dried in the oven overnight at 60°C, and finally used for FTIR testing. FTIR spectra were recorded on a JASCO 6300 spectrophotometer in the solid phase using the KBr pellets technique.

2.7 Cellular Experiments

The human HepG2 cells and LO2 cells were maintained in Dulbecco's modified Eagle medium (DMEM) supplemented with 10% fetal bovine serum, at 37°C, in 5% CO₂. DMEM and fetal bovine serum were ordered from Hyclone (United States). The entire process of cell culture followed American Type Culture Collection instructions.

2.8 Animal Experiments

All animal experiment operations were performed in accordance with the guidelines of the Institutional Animal Care and Use Committee and the care regulations approved

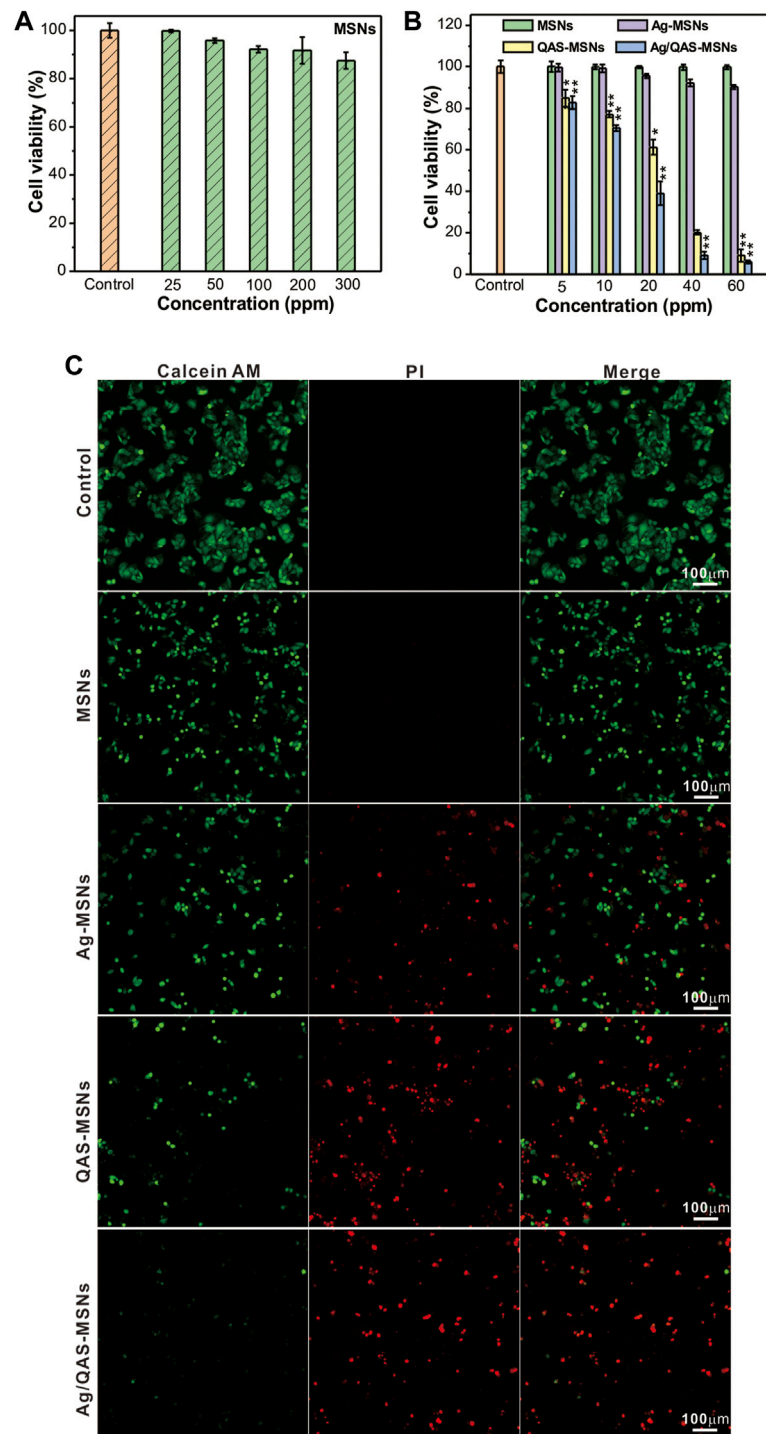


FIGURE 3 | (A,B) Relative survival of HepG2 cells treated with different concentrations of MSNs, Ag-MSNs, QAS-MSNs, and Ag/QAS-MSNs for 24 h. **(C)** Fluorescent images of HepG2 cells incubated with MSNs, Ag-MSNs, QAS-MSNs, and Ag/QAS-MSNs at concentration of 40 ppm. The cells were stained with calcein-AM and PI double fluorescent dye. Green indicates live cells, and red indicates dead cells. All data are presented as the mean of three different measurements \pm SD, asterisks (*) represent the significant difference from the control group using the Bonferroni posttest ($p \leq 0.05$) and asterisks (**) $p < 0.01$.

by the Administrative Committee of Laboratory Animals of Anhui Medical University (No. LLSC20210778). The tumor model was established by the subcutaneous injection of

HepG2 cells (1.0×10^5 cells) into the left axilla of each female Balb/c nude mouse. Tumors were allowed to grow about 50 mm^3 before use.

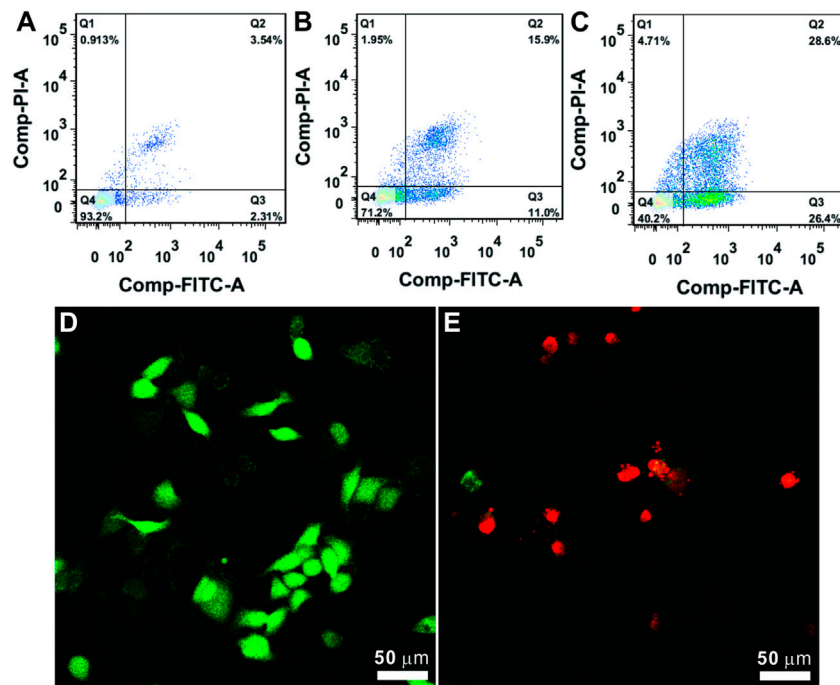


FIGURE 4 | (A–C) Cell apoptosis analysis using the PI/annexin V-FITC double staining method: **(A)** control; **(B)** Ag/QAS-MSNs, 10 ppm; **(C)** Ag/QAS-MSNs, 20 ppm. Q1: necrosis, Q2: late apoptosis, Q3: early apoptosis, Q4: live. **(D,E)** Cell morphology of the dying cells induced by Ag/QAS-MSNs suggested a form of apoptosis: **(D)** control; **(E)** Ag/QAS-MSNs, 20 ppm.

2.9 In Vitro Test of Anticancer Activity

HepG2 cells (1×10^4) were seeded in a 96-well plate for 24 h at 37°C in 5% CO₂. Then, the cells were treated with nanoparticles at determined concentration. After incubation for another 12 h, cell viabilities were tested using the standard MTT [3-(4,5)-dimethylthiazoliazolo-2-yl]-2,5-diphenyltetrazolium bromide) assay.

2.10 Calcein-AM/Propidium Iodide Staining Assay

HepG2 cells were seeded in a 24-well plate. After 24 h of incubation, Ag/QAS-MSNs (10 and 20 ppm) were added to each well for 12 h. Then, the cells were stained with calcein-AM and propidium iodide (PI) double fluorescent dye, washed three times with PBS, and observed in a fluorescence microscope.

2.11 Cell Apoptosis Assay

HepG2 cells were seeded in 12-well plates at a density of 5×10^4 cells/well for 24 h. Ag/QAS-MSNs (10 and 20 ppm) were added to each well. Untreated cells were tested as a negative control. All cells were then washed with PBS and collected by centrifugation. The cells were resuspended in 0.5 ml annexin buffer. Then, all cells were stained with PI and annexin V-FITC containing binding buffer for 15 min and finally detected by flow cytometry.

2.12 In Vivo Anticancer Therapy

HepG2 cells suspended in PBS (100 µL) injected subcutaneously in the left axilla of female Balb/c mice. When the tumor volume was about 50 mm³, the tumor-bearing mice were divided into five

randomized groups ($n = 4$ each group), which were PBS treated (control group), Ag/QAS-MSN treated (nanoparticle dose of 20 mg/kg, Ag dose of 0.84 mg/kg, and QAS dose of 2.02 mg/kg), Ag-MSN treated (Ag dose of 0.84 mg/kg), QAS-MSN treated (QAS dose of 2.02 mg/kg), and MSN treated (nanoparticle dose of 20 mg/kg). Within 15 days of treatment, the nude mice were injected with the nanodrugs twice (the aqueous solution of nanodrugs was directly injected into the tumor site every 7 days). The tumor volumes and body weights were tracked for 15 days to estimate the therapeutic performance. The tumor volume was calculated according to the following formula: tumor volume (V) = (tumor length) \times (tumor width)²/2 (Xu et al., 2022). Furthermore, the major organs of mice (heart, liver, spleen, lung, and kidney) in each group were collected for hematoxylin and eosin (H&E) staining according to the manufacturer's protocols, followed by examination using a digital microscope.

2.13 Test of Antibacterial Activity

The antibacterial activities of the samples were valuated against *E. coli* JM109 and *S. aureus*. These bacteria were cultured in the LB liquid medium at 37°C on a shaker bed until the logarithmic phase [approximately 10^9 colony forming units (CFU)/ml]. Then, 150 µl of 10^7 CFU/ml bacterial suspension containing different concentrations of nanoparticles was added in a 96-well microplate and incubated at 37°C with continuous agitation. At given time intervals, the bacterial growth curve was determined by measuring OD at 600 nm. Control experiments were also performed in the presence of empty MCM-41. Meanwhile, 100 µl suspensions of bacteria with different

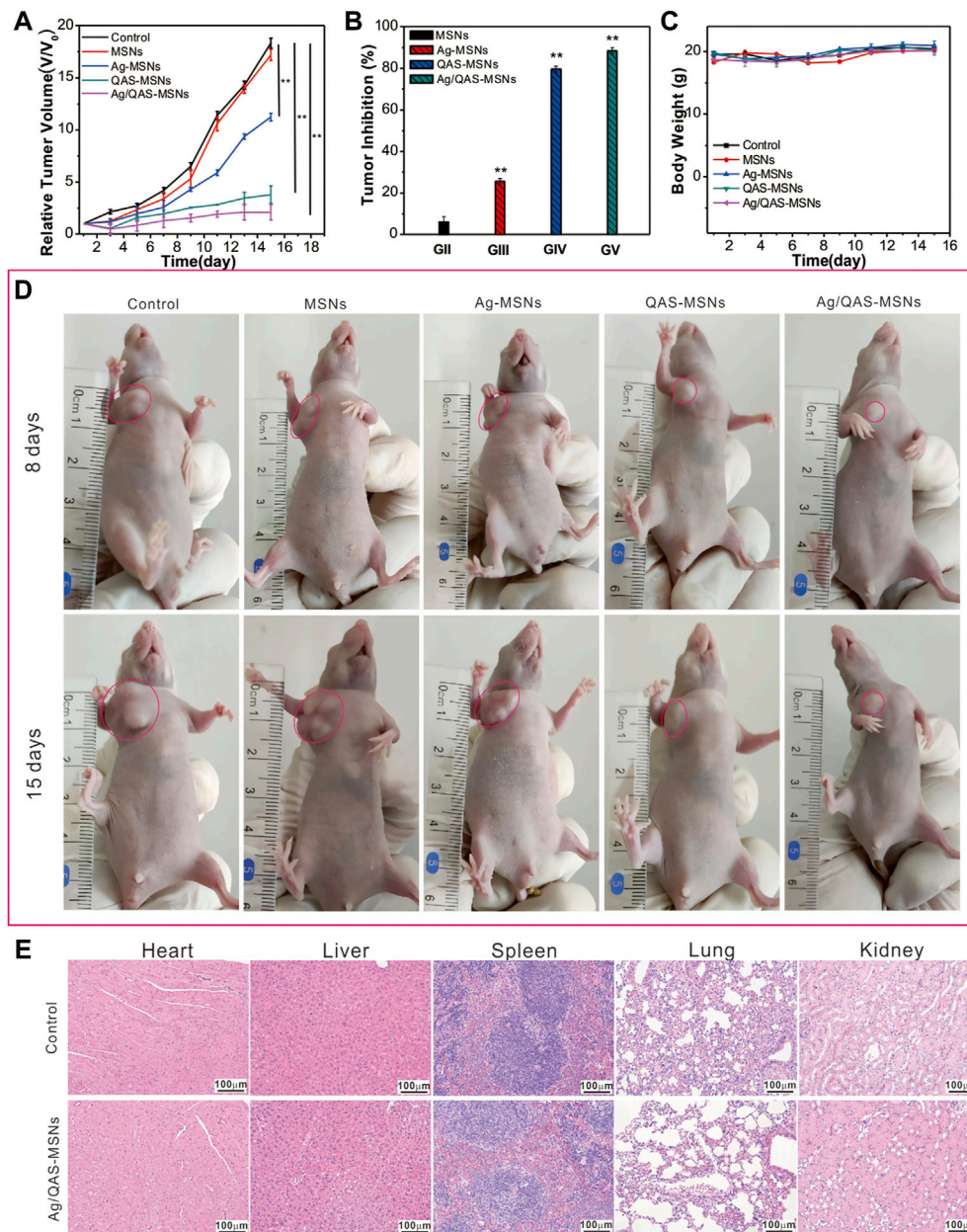


FIGURE 5 | The tumor growth curves (A), the relative tumor volume (B), and the body weights (C) of mice after the treatment with PBS as control, MSNs, Ag-MSNs, QAS-MSNs, and Ag/QAS-MSNs. (D) Representative photos of the tumor-bearing mice treated by five treatment groups after 8 and 15 days (the red circles point to the tumor site). (E) H&E staining images of major organs after treatment with PBS and Ag/QAS-MSNs. All data are presented as the mean of three different measurements \pm SD, asterisks (*) represent the significant difference from the control group using the Bonferroni posttest ($p \leq 0.05$) and asterisks (**) $p < 0.01$.

concentrations of nanoparticles were spread on LB agar plates, and then these agar plates were incubated for 14 h at 37°C.

2.14 Investigation of the Antibacterial Mechanism by SEM

S. aureus (0.5 ml) and *E. coli* bacterial suspensions (0.5 OD) was incubated with Ag/QAS-MSNs (40 ppm) for a given time on a

shaking incubator (180 rpm) at 37°C. The bacteria were harvested by centrifugation and washed with water. Then, the bacteria solution was dropped onto a silicon slice and allowed to dry for SEM observation.

2.15 Statistical Analysis

Data were described as the mean \pm standard deviation, and statistical analysis was performed using one-way analysis and

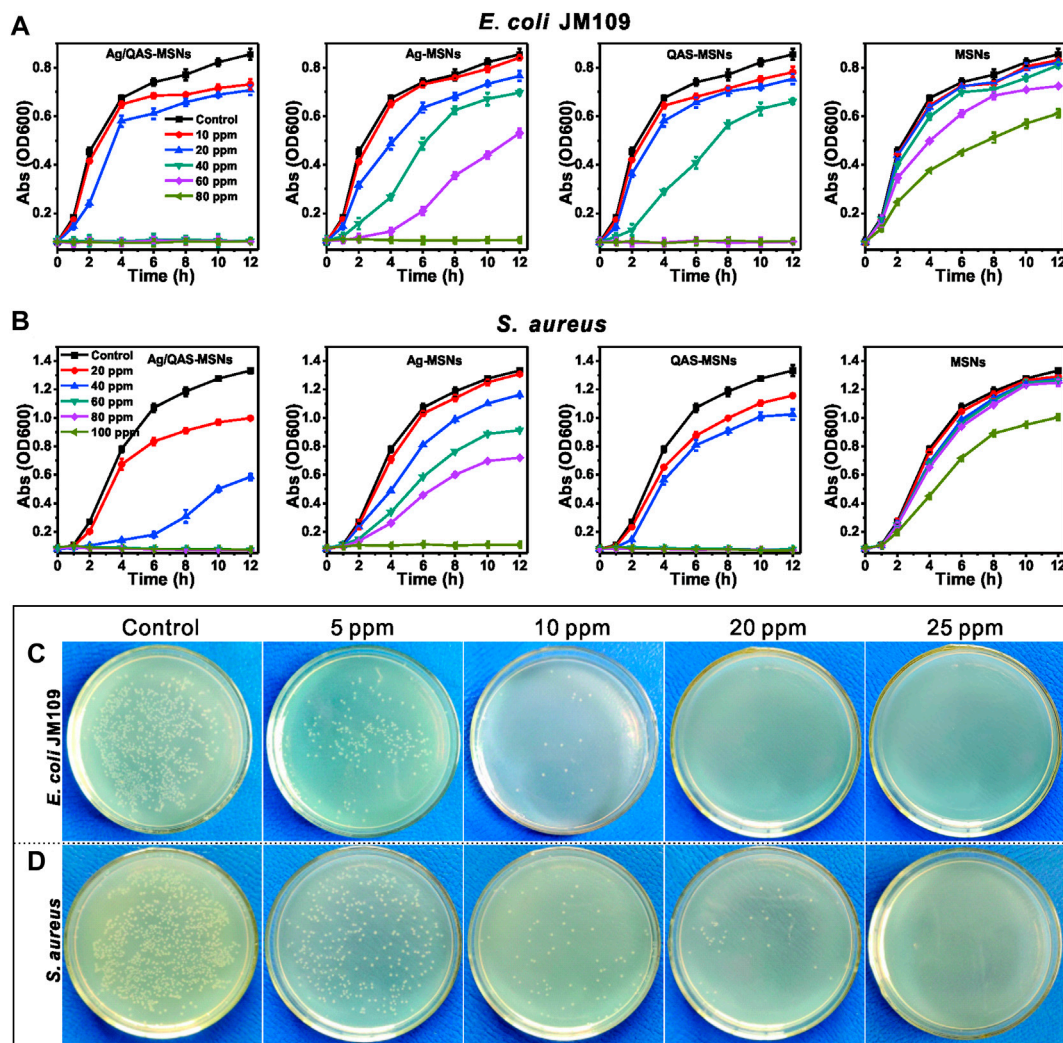


FIGURE 6 | Growth curves of *E. coli* (A) and *S. aureus* (B) in LB liquid medium in the presence of different concentrations of MSNs, Ag-MSNs, QAS-MSNs, and Ag/QAS-MSNs. *E. coli* (C) and *S. aureus* (D) grown on agar plates at different concentrations of Ag/QAS-MSNs.

the Bonferroni posttest. Statistical significance was set at $*p < 0.05$, and significance difference was set at $**p < 0.01$ and $***p < 0.001$.

3 RESULTS AND DISCUSSION

3.1 Synthesis and Characterization of Ag/Quaternary Ammonium Salts Co-Decorated Mesoporous Silica Nanoparticles

Ag/QAS-MSNs were prepared as illustrated in Figure 1A. To effectively encapsulate Ag nanocrystals into the mesostructured silica, TSD was introduced as a chelating agent to capture Ag ions. Then, TEOS and TSD-Ag⁺ complexes were cohydrolyzed to form Ag ions and QAS-MSNs in the presence of QAS, which played the

role of a template and surfactant. Further, formalin was added to reduce Ag ions into Ag NPs. The morphology and particle size of Ag/QAS-MSNs were characterized through TEM. The synthesized Ag/QAS-MSNs were spherical particles 30–80 nm in diameter (Figure 1B and Supplementary Figure S1). Lots of small-sized Ag nanoparticles were firmly attached to the surfaces of the MSNs. From the HRTEM images (Figures 1C, D), a uniform and orderly hexagonal array of mesoporous channel ~2.1 nm in pore diameter, which is the typical mesoporous structure of MCM-41-type MSNs, were observed in Ag/QAS-MSNs, and the diameter of decorated Ag nanoparticles is 2–12 nm. XRD patterns showed that the (111), (200), (220), and (311) planes related to Ag nanoparticles were also found in Ag/QAS-MSNs. In addition, the broad peak at $2\theta = 21$ could be attributed to the amorphous porous silica (Aznar et al., 2009). These results preliminarily prove that Ag/QAS-MSNs were successfully prepared using our one-pot method. Moreover, the

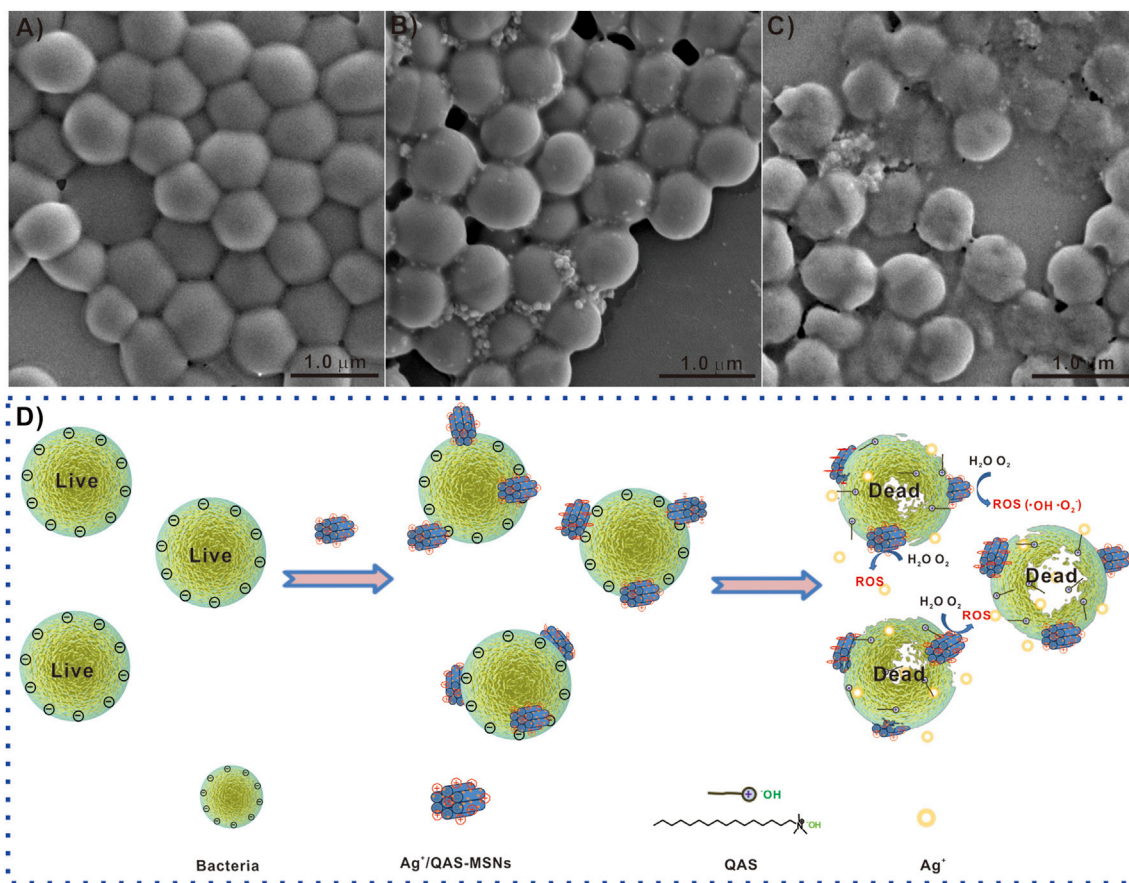


FIGURE 7 | SEM images of *S. aureus* treated with Ag/QAS-MSNs: **(A)** 0 ppm (control), **(B)** 40 ppm for 30 min, and **(C)** 40 ppm for 8 h. **(D)** The possible antibacterial mechanism of Ag/QAS-MSNs.

porosity of MSNs was also investigated by N_2 adsorption/desorption measurements. From **Supplementary Figure S2**, the Brunauer–Emmett–Teller (BET) surface area, pore volume, and pore diameter of the MSNs were $715.5 \text{ m}^2/\text{g}$, $0.64 \text{ m}^3/\text{g}$, and 2.2 nm , respectively.

Figure 2 shows the FTIR spectra of Ag/QAS-MSNs, QAS-MSNs, and Ag-MSNs. The characteristic peak at $1,090 \text{ cm}^{-1}$ was assigned to Si–O–Si stretching vibration of MSNs (Fang et al., 2012), and the characteristic peaks at $2,930$ and $2,850 \text{ cm}^{-1}$ were assigned to C–H stretching vibration coming from QAS and TSD (Fang et al., 2016). All the characteristic adsorption bands were observed in the FTIR spectra of these samples. However, the intensity of the peaks concerning the C–H band in Ag/QAS-MSNs was dramatically higher than that in Ag-MSNs, indicating that the QAS molecules were successfully encapsulated into the mesostructured silica. Thermogravimetric analysis (TGA) was further used for quantitative analysis of the amounts of QAS in Ag/QAS-MSNs. From **Figure 2B**, it was obvious that Ag/QAS-MSNs have two weight loss stages when heated in air. A weight loss below 400°C might be due to the release of high-boiling solvent absorbed on the nanoparticles' surface, while a further weight loss when temperature is up to 400°C probably corresponded to the burning of the QAS. Based on the TGA curves of Ag/QAS-MSNs and Ag-MSNs, the

encapsulation of QAS in Ag/QAS-MSNs was calculated as $10.1 \text{ wt}\%$. Additionally, the loading amount of Ag in Ag/QAS-MSNs determined by ICP-MS was $\sim 4.2 \text{ wt}\%$ (**Supplementary Table S1**).

3.2 *In Vitro* Anticancer Activity of Ag/Quaternary Ammonium Salts Co-Decorated MSNs

In order to investigate the cytotoxicity of the MSN vehicles *in vitro*, HepG2 cells and LO2 cells (normal human live cells) were incubated with different concentrations of MSNs and determined using a standard MTT assay (**Figure 3** and **Supplementary Figure S2**). As shown in **Figure 3A**, no obvious cytotoxicity was detected for the MSN vehicles without QAS and Ag NP loading even after 24-h incubation at the concentration of 300 ppm , which suggested the biocompatibility of the MCM-41-type vehicles. Results from **Figure 3B** showed that the cell viabilities exhibited a marked decline in a dose-dependent manner in the presence of Ag/QAS-MSNs, QAS-MSNs, and Ag-MSNs, and Ag/QAS-MSNs showed higher antitumor effect than QAS-MSNs and Ag-MSNs at the same condition. For instance, the viability of cells treated with Ag/QAS-MSNs at the concentration of 40 ppm [QAS: 4.04 ppm ($10.1 \text{ wt}\%$) silver: 1.68 ppm ($4.2 \text{ wt}\%$)] was decreased to 9.1% , while that of cells

treated with QAS-MSNs (QAS: 4.04 ppm) and Ag-MSNs (Ag: 1.68 ppm) were only 20.2 and 92.2%, respectively. It was intuitively observed, using the calcein-AM/PI staining double staining method, that cells incubated with MSNs mainly displayed green fluorescence (color in green indicates live cells, and color in red indicates dead cells). The Ag-MSNs group showed a small amount of red fluorescent cells, while both the QAS-MSNs and Ag/QAS-MSNs groups exhibited almost dead cells, which was consistent with the data of CCK-8 assay.

Further, the possible Ag/QAS-MSN-induced cell death mechanism was investigated by the flow cytometry analysis. Results shown in **Figure 4C** indicated that cell populations in early and late apoptosis were increased dose-dependently in the presence of Ag/QAS-MSNs. As seen, the percentage in apoptosis for the Ag/QAS-MSN-treated cells increased from 26.9% (early and late apoptosis) at 10 ppm to 55% at 20 ppm. From the fluorescence images, the green fluorescence indicates no morphological changes (control cells). The cells treated with Ag/QAS-MSNs exhibited significant changes including cell shrinkage, cell membrane blebbing, DNA fragmentation of apoptotic bodies. These results demonstrate that cell death induced by Ag/QAS-MSNs is mainly caused by apoptosis.

3.3 *In Vivo* Anticancer Activity and Biosafety of Ag/Quaternary Ammonium Salts Co-Decorated Mesoporous Silica Nanoparticles

The HepG2 tumor-bearing mice are randomly separated into five groups, namely, PBS, MSNs, Ag-MSNs, QAS-MSNs, and Ag/QAS-MSNs. As illustrated in **Figure 5A**, the relative tumor sizes decreased considerably upon treatment with Ag/QAS-MSNs compared with those upon treatment with PBS, MSNs, Ag-MSNs, and QAS-MSNs. About 88.5% of tumor inhibition ratio was shown by the treatment with Ag/QAS-MSNs for 15 days (**Figure 5B**), whereas Ag-MSNs and QAS-MSNs treatments achieved only 25.7 and 79.7% of tumor inhibition ratio, respectively. In agreement with these results, the representative images of tumor-bearing mice of each group are shown in **Figure 5D**. During 15-day treatments, all groups did not show significant body weight changes. H&E staining of the major organs treated with PBS (control group), MSNs, Ag-MSNs, QAS-MSNs, and Ag/QAS-MSNs exhibited no histopathological abnormalities, which indicated that the above nanomaterials nearly had no side effects on the health of the mice (**Figure 5E** and **Supplementary Figure S4**). Therefore, these results revealed that Ag/QAS-MSNs can be considered a promising anticancer agent in tumor treatment without producing toxicity.

3.4 *In Vitro* Antibacterial Activity and Its Mechanism

The antibacterial activity of the nanomaterials was evaluated against selected pathogenic Gram-negative (*E. coli* JM109) and Gram-positive strains (*S. aureus*) in both liquid media and LB agar plates. The bacterial strains were incubated with MSNs, Ag-MSNs, bare Ag NPs, pure QAS, QAS-MSNs and Ag/QAS-MSNs at the same equivalent concentrations. The results demonstrated that Ag/QAS-MSNs

displayed a strongest antibacterial activity when compared with Ag-MSNs, QAS-MSNs, bare Ag NPs, and pure QAS (**Figure 6** and **Supplementary Figure S5**). As can be seen from **Figure 6A**, the proliferation of *E. coli* was completely inhibited in the presence Ag/QAS-MSNs at the concentration of 40 ppm, whereas no significant antibacterial activity was observed in the groups of MSNs, Ag-MSNs, and QAS-MSNs. In the case of *S. aureus* (**Figure 6B**), 60 ppm of Ag/QAS-MSNs was needed to completely suppress bacterial growth in liquid media, which suggested that the Gram-positive *S. aureus* was more tolerant than the Gram-negative *E. coli* to Ag/QAS-MSNs. This resistance may be due to the thicker cell wall and different chemical components of Gram-positive bacteria (Buckley et al., 2010; Fang et al., 2014). Additionally, QAS-MSNs appeared to have a slightly higher antibacterial effect against the two pathogenic bacteria than did Ag-MSNs at all test concentrations. **Figures 6C, D** depict the formation of bacterial colonies on the control and Ag/QAS-MSNs after 14-h incubation. It was obviously seen that Ag/QAS-MSNs can effectively inhibit bacterial growth in a concentration-dependent manner. The growth of bacterial colonies was completely prevented, when the concentration of Ag/QAS-MSNs was increased to 20 ppm for *E. coli* and 25 ppm for *S. aureus*, respectively. Hence, the prepared Ag/QAS-MSNs can act as an effective antibacterial agent.

To further investigate the antibacterial mechanism of Ag/QAS-MSNs, the mixture of *S. aureus* and nanomaterials was used for SEM analysis at different incubation times. After incubation for 30 min, SEM images (**Figure 7B** and **Supplementary Figure S7**) reveal that *S. aureus* still maintained intact cell wall structure, and lots of Ag/QAS-MSNs adhered to the outer membrane of the cells. This was because the negatively charged bacterial cell wall can easily adhere to materials carrying positive charges (**Supplementary Figure S8**) (Fang et al., 2017; Hu et al., 2020). However, with the extension of the incubation times (**Figure 7C**), destruction and degradation of the cell membrane were observed, and most bacterial cells had no intact cell morphology indicating dead cells. These phenomena propose that the possible antibacterial mechanisms are as follows (**Figure 7D**): First, Ag/QAS-MSNs with positive charges adhere to the negatively charged bacterial cell wall via electrostatic interaction and cause injury to the cytomembrane (Hayden et al., 2012; Chen et al., 2014). Subsequently, the sustainable release of Ag ions and QAS from Ag/QAS-MSNs can directly lead to membrane damage and cell death. However, the Ag ions may also generate reactive oxygen species inducing membrane lipid peroxidation, DNA damage, and protein denaturation (Eckhardt et al., 2013).

4 CONCLUSION

In summary, we describe the synthesis of Ag/QAS-MSNs via the one-pot co-condensation method for anti-bacteria and *in vivo* tumor treatment. Our experimental results demonstrated that Ag/QAS-MSNs possess excellent antibacterial activity and anticancer property. The excellent anticancer and antibacterial activity of Ag/QAS-MSNs could be ascribed to the synergistic effect of Ag ions and QAS. Hence, we state that Ag/QAS-MSNs can emerge as promising agents for effective treatment of tumors and the related bacterial infections.

DATA AVAILABILITY STATEMENT

The original contributions presented in the study are included in the article/**Supplementary Material**, and further inquiries can be directed to the corresponding authors.

ETHICS STATEMENT

The animal study was reviewed and approved by the Administrative Committee of Laboratory Animals of Anhui Medical University (No. LLSC20210778).

AUTHOR CONTRIBUTIONS

Designed the experiments: WF and TZ. Performed the experiments: HZ, JX, XZ, DZ, and WS. Analyzed the data: WF, HZ, and TW. Contributed to the writing of the manuscript: WF, TZ, and HZ. Revised the manuscript: WF, TZ, and HZ. All authors reviewed the manuscript.

FUNDING

This work was supported by the National Natural Science Foundation of China (No. 21703255, TZ), the Natural Science Foundation of Anhui Province (No. 1908085MB47, WF; No.

1708085MB35, TZ), the Key Projects of Anhui Province University Outstanding Youth Talent Support Program (No. gxyqZD2018021, WF), the Anhui Province Overseas Students Innovation Project Selection Funding Program-Key Project (No. 2021LCX003, TZ), and the Anhui Province Innovation and Entrepreneurship Training Program for College Students (No. S202110366063, WF).

ACKNOWLEDGMENTS

We thank the National Natural Science Foundation of China (No. 21703255), the Natural Science Foundation of Anhui Province (No. 1908085MB47, 1708085MB35), the Key Projects of Anhui Province University Outstanding Youth Talent Support Program (No. gxyqZD2018021), the Anhui Province Overseas Students Innovation Project Selection Funding Program-Key Project (No. 2021LCX003) for the financial support, and the Anhui Province Innovation and Entrepreneurship Training Program for College Students (No. S202110366063).

SUPPLEMENTARY MATERIAL

The Supplementary Material for this article can be found online at: <https://www.frontiersin.org/articles/10.3389/fbioe.2022.875317/full#supplementary-material>

REFERENCES

- Ahn, E.-Y., and Park, Y. (2020). Anticancer Prospects of Silver Nanoparticles Green-Synthesized by Plant Extracts. *Mater. Sci. Eng. C* 116, 111253. doi:10.1016/j.msec.2020.111253
- Aznar, E., Marcos, M. D., Martínez-Máñez, R., Sancenón, F., Soto, J., Amorós, P., et al. (2009). pH- and Photo-Switched Release of Guest Molecules from Mesoporous Silica Supports. *J. Am. Chem. Soc.* 131, 6833–6843. doi:10.1021/ja810011p
- Banerjee, I., Pangule, R. C., and Kane, R. S. (2011). Antifouling Coatings: Recent Developments in the Design of Surfaces that Prevent Fouling by Proteins, Bacteria, and Marine Organisms. *Adv. Mat.* 23, 690–718. doi:10.1002/adma.201001215
- Bayda, S., Amadio, E., Cailotto, S., Frión-Herrera, Y., Perosa, A., and Rizzolio, F. (2021). Carbon Dots for Cancer Nanomedicine: A Bright Future. *Nanoscale Adv* 3 (2021), 5183–5221. doi:10.1039/d1na00036e
- Bi, X., Bai, Q., Liang, M., Yang, D., Li, S., and Wang, L. (2022). Silver Peroxide Nanoparticles for Combined Antibacterial Sonodynamic and Photothermal Therapy. *Small* 18 (2022), 2104160. doi:10.1002/smll.202104160
- Buckley, J. J., Lee, A. F., Olivi, L., and Wilson, K. (2010). Hydroxyapatite Supported Antibacterial Ag₃PO₄ Nanoparticles. *J. Mat. Chem.* 20, 8056–8063. doi:10.1039/c0jm01500h
- Bullman, S., Pedamallu, C. S., Sicinska, E., Clancy, T. E., Zhang, X., Cai, D., et al. (2017). Analysis of Fusobacterium Persistence and Antibiotic Response in Colorectal Cancer. *Science* 358, 1443–1448. doi:10.1126/science.aal5240
- Chen, G., Li, Z., Wang, X., Xie, L., Qi, Q., and Fang, W. (2014). Preparation of CTAB-Loaded Magnetic Nanospheres for Rapid Bacterial Capture and Decantation. *Mater. Lett.* 134, 290–294. doi:10.1016/j.matlet.2014.07.100
- Chen, X., Huang, L., Jia, Y., Hu, R., Gao, M., Ren, L., et al. (2020). AIE-Based Theranostic Probe for Sequential Imaging and Killing of Bacteria and Cancer Cells. *Adv. Opt. Mat.* 8, 1902191. doi:10.1002/adom.201902191
- Chu, M., Shao, Y., Peng, J., Dai, X., Li, H., Wu, Q., et al. (2013). Near-infrared Laser Light Mediated Cancer Therapy by Photothermal Effect of Fe₃O₄ Magnetic Nanoparticles. *Biomaterials* 34, 4078–4088. doi:10.1016/j.biomaterials.2013.01.086
- Deshmukh, S. P., Patil, S. M., Mullani, S. B., and Delekar, S. D. (2019). Silver Nanoparticles as an Effective Disinfectant: A Review. *Mater. Sci. Eng. C* 97, 954–965. doi:10.1016/j.msec.2018.12.102
- Dewerd, S. (2015). Microbiome: Microbial Mystery. *Nature* 521, S10–S11. doi:10.1038/521s10a
- Eckhardt, S., Brunetto, P. S., Gagnon, J., Priebe, M., Giese, B., and Fromm, K. M. (2013). Nanobio Silver: Its Interactions with Peptides and Bacteria, and its Uses in Medicine. *Chem. Rev.* 113, 4708–4754. doi:10.1021/cr300288v
- Eid, A. M., Fouda, A., Niedbala, G., Hassan, S. E.-D., Salem, S. S., Abdo, A. M., et al. (2020). Endophytic Streptomyces Laurentii Mediated Green Synthesis of Ag-NPs with Antibacterial and Anticancer Properties for Developing Functional Textile Fabric Properties. *Antibiotics* 9, 641. doi:10.3390/antibiotics9100641
- Fang, W., Han, C., Zhang, H., Wei, W., Liu, R., and Shen, Y. (2016). Preparation of Amino-Functionalized Magnetic Nanoparticles for Enhancement of Bacterial Capture Efficiency. *RSC Adv.* 6, 67875–67882. doi:10.1039/c6ra13070d
- Fang, W., Yang, J., Gong, J., and Zheng, N. (2012). Photo- and pH-Triggered Release of Anticancer Drugs from Mesoporous Silica-Coated Pd@Ag Nanoparticles. *Adv. Funct. Mat.* 22, 842–848. doi:10.1002/adfm.201101960
- Fang, W., Zhang, H., Wang, X., Wei, W., Shen, Y., Yu, J., et al. (2017). Facile Synthesis of Tunable Plasmonic Silver Core/magnetic Fe₃O₄ Shell Nanoparticles for Rapid Capture and Effective Photothermal Ablation of Bacterial Pathogens. *New J. Chem.* 41, 10155–10164. doi:10.1039/c7nj02071f
- Fang, W., Zheng, J., Chen, C., Zhang, H., Lu, Y., Ma, L., et al. (2014). One-pot Synthesis of Porous Fe₃O₄ Shell/silver Core Nanocomposites Used as Recyclable Magnetic Antibacterial Agents. *J. Magnetism Magnetic Mater.* 357, 1–6. doi:10.1016/j.jmmm.2014.01.024
- Galhano, J., Marcelo, G. A., Duarte, M. P., and Oliveira, E. (2022). Ofloxacin@Doxorubicin-Epirubicin Functionalized MCM-41 Mesoporous Silica-Based

- Nanocarriers as Synergistic Drug Delivery Tools for Cancer Related Bacterial Infections. *Bioorg. Chem.* 118, 105470. doi:10.1016/j.bioorg.2021.105470
- Geller, L. T., Barzily-Rokni, M., Danino, T., Jonas, O. H., Shental, N., Nejman, D., et al. (2017). Potential Role of Intratumor Bacteria in Mediating Tumor Resistance to the Chemotherapeutic Drug Gemcitabine. *Science* 357, 1156–1160. doi:10.1126/science.aah5043
- Harper, K. (2019). Lung Microbiota Promote Lung Cancer. *Cancer Discov.* 9, 458. doi:10.1158/2159-8290.cd-nb2019-019
- Hayden, S. C., Zhao, G., Saha, K., Phillips, R. L., Li, X., Miranda, O. R., et al. (2012). Aggregation and Interaction of Cationic Nanoparticles on Bacterial Surfaces. *J. Am. Chem. Soc.* 134, 6920–6923. doi:10.1021/ja301167y
- He, D., Tan, Y., Li, P., Luo, Y., Zhu, Y., Yu, Y., et al. (2021). Surface Charge-Convertible Quaternary Ammonium Salt-Based Micelles for *In Vivo* Infection Therapy. *Chin. Chem. Lett.* 32, 1743–1746. doi:10.1016/j.ccl.2020.12.034
- He, Q., Gao, Y., Zhang, L., Zhang, Z., Gao, F., Ji, X., et al. (2011). A pH-Responsive Mesoporous Silica Nanoparticles-Based Multi-Drug Delivery System for Overcoming Multi-Drug Resistance. *Biomaterials* 32, 7711–7720. doi:10.1016/j.biomaterials.2011.06.066
- He, Q., Shi, J., Chen, F., Zhu, M., and Zhang, L. (2010). An Anticancer Drug Delivery System Based on Surfactant-Templated Mesoporous Silica Nanoparticles. *Biomaterials* 31, 3335–3346. doi:10.1016/j.biomaterials.2010.01.015
- Hu, D., Deng, Y., Jia, F., Jin, Q., and Ji, J. (2020). Surface Charge Switchable Supramolecular Nanocarriers for Nitric Oxide Synergistic Photodynamic Eradication of Biofilms. *ACS Nano* 14, 347–359. doi:10.1021/acsnano.9b05493
- Huang, C.-C., Chang, P.-Y., Liu, C.-L., Xu, J.-P., Wu, S.-P., and Kuo, W.-C. (2015). New Insight on Optical and Magnetic Fe₃O₄ Nanoclusters Promising for Near Infrared Theranostic Applications. *Nanoscale* 7, 12689–12697. doi:10.1039/c5nr03157e
- Hsu, I. L., Yeh, F. H., Chin, Y. C., Cheung, C. I., Chia, Z. C., Yang, L. X., et al. (2021). Multiplex Antibacterial Processes and Risk in Resistant Phenotype by High Oxidation-State Nanoparticles: New Killing Process and Mechanism Investigations. *Chem. Eng. J.* 409, 128266. doi:10.1016/j.cej.2020.128266
- Ito, E., Yip, K. W., Katz, D., Fonseca, S. B., Hedley, D. W., Chow, S., et al. (2009). Potential Use of Cetrimonium Bromide as an Apoptosis-Promoting Anticancer Agent for Head and Neck Cancer. *Mol. Pharmacol.* 76, 969–983. doi:10.1124/mol.109.055277
- Kang, M., Kwok, R. T. K., Wang, J., Zhang, H., Lam, J. W. Y., Li, Y., et al. (2018). A Multifunctional Luminogen with Aggregation-Induced Emission Characteristics for Selective Imaging and Photodynamic Killing of Both Cancer Cells and Gram-Positive Bacteria. *J. Mat. Chem. B* 6, 3894–3903. doi:10.1039/c8tb00572a
- Kwasniewska, D., Chen, Y. L., and Wiczczyk, D. (2020). Biological Activity of Quaternary Ammonium Salts and Their Derivatives. *Pathogens* 9, 459. doi:10.3390/pathogens9060459
- Liang, Q., Chiu, J., Chen, Y., Huang, Y., Higashimori, A., Fang, J., et al. (2017). Fecal Bacteria Act as Novel Biomarkers for Noninvasive Diagnosis of Colorectal Cancer. *Clin. Cancer Res.* 23, 2061–2070. doi:10.1158/1078-0432.ccr-16-1599
- Lima-Sousa, R., de Melo-Diogo, D., Alves, C. G., Cabral, C. S. D., Miguel, S. P., Mendonça, A. G., et al. (2020). Injectable *In Situ* Forming Thermo-Responsive Graphene Based Hydrogels for Cancer Chemo-Photothermal Therapy and NIR Light-Enhanced Antibacterial Applications. *Mater. Sci. Eng. C* 117, 111294. doi:10.1016/j.msec.2020.111294
- Meena, R., Kumar, S., Kumar, R., Gaharwar, U. S., and Rajamani, P. (2017). PLGA-CTAB Curcumin Nanoparticles: Fabrication, Characterization and Molecular Basis of Anticancer Activity in Triple Negative Breast Cancer Cell Lines (MDA-MB-231 Cells). *Biomed. Pharmacother.* 94, 944–954. doi:10.1016/j.biopha.2017.07.151
- Montalvo-Quiros, S., Aragonese-Cazorla, G., Garcia-Alcalde, L., Vallet-Regí, M., González, B., and Luque-García, J. L. (2019). Cancer Cell Targeting and Therapeutic Delivery of Silver Nanoparticles by Mesoporous Silica Nanocarriers: Insights into the Action Mechanisms Using Quantitative Proteomics. *Nanoscale* 11, 4531–4545. doi:10.1039/c8nr07667g
- Oblak, E., Piecuch, A., Rewak-Soroczynska, J., and Paluch, E. (2019). Activity of Gemini Quaternary Ammonium Salts against Microorganisms. *Appl. Microbiol. Biotechnol.* 103, 625–632. doi:10.1007/s00253-018-9523-2
- Oliveira, R. d. S., Camilo, F. F., and Bizeto, M. A. (2016). Evaluation of the Influence of Sulfur-Based Functional Groups on the Embedding of Silver Nanoparticles into the Pores of MCM-41. *J. Solid State Chem.* 235, 125–131. doi:10.1016/j.jssc.2015.12.024
- Shen, S., Xu, X., Lin, S., Zhang, Y., Liu, H., Zhang, C., et al. (2021). A Nanotherapeutic Strategy to Overcome Chemotherapeutic Resistance of Cancer Stem-like Cells. *Nat. Nanotechnol.* 16, 104–113. doi:10.1038/s41565-020-00793-0
- Siegel, R. L., Miller, K. D., and Jemal, A. (2020). Cancer Statistics, 2020. *CA A Cancer J. Clin.* 70, 7–30. doi:10.3322/caac.21590
- Song, Y., Cai, L., Tian, Z., Wu, Y., and Chen, J. (2020). Phytochemical Curcumin-Coformulated, Silver-Decorated Melanin-like Polydopamine/Mesoporous Silica Composites with Improved Antibacterial and Chemotherapeutic Effects against Drug-Resistant Cancer Cells. *ACS Omega* 5, 15083–15094. doi:10.1021/acsomega.0c00912
- Tan, G., Zhong, Y., Yang, L., Jiang, Y., Liu, J., and Ren, F. (2020). A Multifunctional MOF-Based Nanohybrid as Injectable Implant Platform for Drug Synergistic Oral Cancer Therapy. *Chem. Eng. J.* 390, 124446. doi:10.1016/j.cej.2020.124446
- Tang, M., Zhang, P., Liu, J., Long, Y., Cheng, Y., and Zheng, H. (2020). Cetyltrimethylammonium Chloride-Loaded Mesoporous Silica Nanoparticles as a Mitochondrion-Targeting Agent for Tumor Therapy. *RSC Adv.* 10, 17050–17057. doi:10.1039/d0ra02023k
- Tang, S., and Zheng, J. (2018). Antibacterial Activity of Silver Nanoparticles: Structural Effects. *Adv. Healthc. Mat.* 7, 1701503. doi:10.1002/adhm.201701503
- Te, W. C., and Wei, S. H. (2022). Tannic Acid-Induced Interfacial Ligand-To-Metal Charge Transfer and the Phase Transformation of Fe₃O₄ Nanoparticles for the Photothermal Bacteria Destruction. *Chem. Eng. J.* 428, 131237. doi:10.1016/j.cej.2021.131237
- Tian, Y., Qi, J., Zhang, W., Cai, Q., and Jiang, X. (2014). Facile, One-Pot Synthesis, and Antibacterial Activity of Mesoporous Silica Nanoparticles Decorated with Well-Dispersed Silver Nanoparticles. *ACS Appl. Mat. Interfaces* 6, 12038–12045. doi:10.1021/am5026424
- Wallace, B. D., Wang, H., Lane, K. T., Scott, J. E., Orans, J., Koo, J. S., et al. (2010). Alleviating Cancer Drug Toxicity by Inhibiting a Bacterial Enzyme. *Science* 330, 831–835. doi:10.1126/science.1191175
- Xu, J., Zhang, H., Zhang, Y., Zhang, X., Wang, T., Hong, S., et al. (2022). Controllable Synthesis of Variable-Sized Magnetic Nanocrystals Self-Assembled into Porous Nanostructures for Enhanced Cancer Chemo-Ferroptosis Therapy and MR Imaging. *Nanoscale Adv* 4 (3), 782–791. doi:10.1039/d1na00767j
- Xu, L., Wang, Y.-Y., Huang, J., Chen, C.-Y., Wang, Z.-X., and Xie, H. (2020). Silver Nanoparticles: Synthesis, Medical Applications and Biosafety. *Theranostics* 10, 8996–9031. doi:10.7150/thno.45413
- Youbare, S., Chang, T.-K., Tan, S.-H., Kuo, J.-C., Hsu, P.-H., Su, C.-Y., et al. (2019). Antimicrobial Gold Nanoclusters: Recent Developments and Future Perspectives. *Int. J. Mol. Sci.* 20, 2924. doi:10.3390/ijms20122924
- Yu, T., Guo, F., Yu, Y., Sun, T., Ma, D., Han, J., et al. (2017). Fusobacterium Nucleatum Promotes Chemoresistance to Colorectal Cancer by Modulating Autophagy. *170*, 548–563. doi:10.1016/j.cell.2017.07.008
- Yu, W. C., and Chi, M. L. (2020). Amino-modified Graphene Oxide Nanoplatelets for Photo-Thermal and Antibacterial Capability. *Surf. Coat. Tech.* 385, 125441. doi:10.1016/j.surfcoat.2020.125441

Conflict of Interest: The authors declare that the research was conducted in the absence of any commercial or financial relationships that could be construed as a potential conflict of interest.

Publisher's Note: All claims expressed in this article are solely those of the authors and do not necessarily represent those of their affiliated organizations or those of the publisher, the editors, and the reviewers. Any product that may be evaluated in this article, or claim that may be made by its manufacturer, is not guaranteed or endorsed by the publisher.

Copyright © 2022 Zhang, Xu, Zhang, Wang, Zhou, Shu, Zhao and Fang. This is an open-access article distributed under the terms of the Creative Commons Attribution License (CC BY). The use, distribution or reproduction in other forums is permitted, provided the original author(s) and the copyright owner(s) are credited and that the original publication in this journal is cited, in accordance with accepted academic practice. No use, distribution or reproduction is permitted which does not comply with these terms.